Entanglement between low- and high-lying atomic spin waves

D. S. Ding,[*] K. Wang, W. Zhang, S. Shi, M. X. Dong, Y. C. Yu, Z. Y. Zhou, B. S. Shi,[†] and G. C. Guo

Key Laboratory of Quantum Information, University of Science and Technology of China, Hefei, Anhui 230026, China
and Synergetic Innovation Center of Quantum Information and Quantum Physics, University of Science and Technology of China,
Hefei, Anhui 230026, China

Establishing a quantum interface between different physical systems is of special importance for developing the practical versatile quantum networks. Entanglement between low- and high-lying atomic spin waves is essential for building up Rydberg-based quantum information engineering, which is also helpful to study the dynamics behavior of entanglement under external perturbations. Here, we report on the successful storage of a single photon as a high-lying atomic spin wave in a quantum regime. By storing a K-vector entanglement between a single photon and low-lying spin wave, we experimentally realize the entanglement between low- and high-lying atomic spin waves in two separated atomic systems. This makes our experiment a primary demonstration of Rydberg quantum memory of entanglement, representing a primary step toward the construction of a hybrid quantum interface.

As a unique physical phenomenon in quantum mechanics, entanglement entails states of two or more objects that when separated cannot be described independently, a notion quite counterintuitive in classical physics. It plays a vital role in quantum information engineering with separated entangled systems, offers a great resource not available within classical counterparts, and also facilitates the study of many fundamental quantum physics. In quantum information science, entanglement between separated physical systems is an indispensable resource in establishing distributed correlation across network nodes [1].

As the blockade effect of the large dipole moment of a highly excited Rydberg atom in a confined volume [2,3], a high-lying atomic spin wave from single collective Rydberg excitation has been proposed as a potential candidate for realizing quantum computing [4,5]. The interacting strength between two Rydberg atoms can be turned on and off with a contrast of 12 orders of magnitude by preparing the atoms to Rydberg states or not [6], which results in a significant advantage in realizing a controlled-NOT (CNOT) gate [7]. Moreover, the high-lying atomic spin wave is central to many other interesting applications, such as efficient single-photon generation [8], exploration of the attractive interaction between single photons [9], preparation of entanglement between light and atomic excitations [10], all-optical switching operating using a single photon [11,12], and studying nonequilibrium phase transitions with many-body physics [13,14]. A low-lying atomic spin wave consisting of metastable levels is suitable for quantum memory because of its long coherence time, a major barrier to long-distance quantum communication [15–22]. Regarded as disparate quantum systems, connecting the low- and high-lying atomic spin waves is crucially important in establishing long-distance quantum communication [1,15] and distributed quantum computation [23,24]. In addition, developing a quantum link between low- and high-lying atomic spin waves would make quantum networks work with superior scaling properties and have other

advantages [6], such as the MHz-rate gate operations and more tolerance to some critical parameters, including weak dependence on atomic motion and independence on the blockade shift. Alternatively, such entanglement is very promising for studying the dynamics behavior of entanglement under external perturbations, such as microwave and rf dressing. Demonstrating an entanglement between the two is therefore interesting and merits investigation.

In this paper, we report the development of a hybrid quantum link between two distant separated atomic ensembles through exciting a single photon as a high-lying atomic spin wave. We first establish the entanglement between an anti-Stokes photon and a low-lying spin wave of one cold-atomic ensemble by spontaneous Raman scattering (SRS). Next, we send this anti-Stokes photon to excite a high-lying atomic spin wave in another cold-atomic ensemble. Via special designed interferometers, the low- and high-lying atomic spin waves are entangled in K-vector spaces. We demonstrate this entanglement by mapping them into two photons and checking their entanglement. We find that the Clauser-Horne-Shimony-Holt (CHSH) inequality is violated by more than nine standard deviations.

The medium for hybrid interface is optically thick ensembles of ^{85}Rb atoms trapped in two two-dimensional magneto-optical traps labeled MOT A and MOT B [Fig. 1(a)]. The temperature of the atomic cloud in each is $\sim$200 μK and its size is $2 \times 2 \times 30$ mm^3 [25]. The optical depths are 20 and 10, respectively. The hybrid quantum link involves two procedures: (a) preparing an entanglement between a single photon and the low-lying atomic spin wave by SRS in MOT A, and (b) storing a single photon as a high-lying atomic spin wave through EIT. The experiment was run periodically with a magneto-optical trap (MOT) trapping time of 7.5 ms and an experiment operating time of 1.5 ms, which contained 3000 operation cycles of storage, and each cycle a period of 500 ns [see time sequence in Fig. 1(c)]. Another 1 ms was used to prepare atoms to the initial atomic state $|3\rangle$ in MOT A, and state $|1\rangle$ in MOT B.

The signal-1 photon is prepared by an atomic SRS process, which is correlated with the low-lying atomic spin wave $|a_{\text{low}}\rangle = 1/\sqrt{m} \sum_{i=1}^{m} e^{i\mathbf{k}_S \cdot \mathbf{r}_i} |3\rangle_1 \cdots |1\rangle_i \cdots |3\rangle_m$ in the
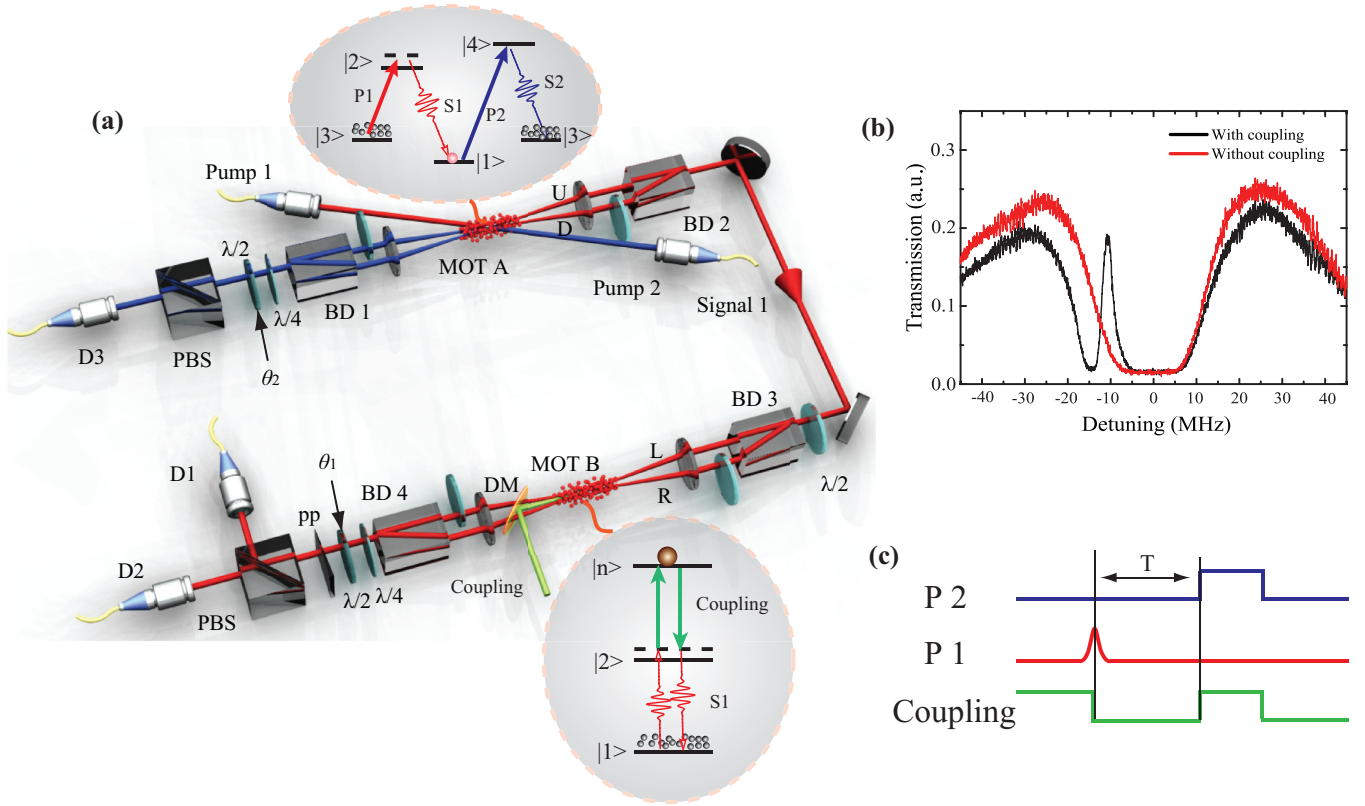
FIG. 1. (a) Experimental setup and energy-level diagrams. The rubidium energy levels (dashed ellipses) were used in storing the signal-1 photon. $|1\rangle$ and $|3\rangle$ are atomic levels of $5S_{1/2}$ ($F = 2$) and $5S_{1/2}$ ($F = 3$). $|2\rangle$ and $|4\rangle$ are $5P_{1/2}$ ($F = 3$) and $5P_{3/2}$ ($F = 3$), respectively. $|n\rangle$ represents Rydberg state $nD_{3/2}$. DM: dichroic mirror. P_1, P_2: pumps 1 and 2. S_1, S_2: signals 1 and 2. M: mirror. BD: beam displacer. $\lambda/2$: half-wave plate. $\lambda/4$: quarter-wave plate. pp: the inserted phase plate. D1–D3: single-photon detectors. $\vartheta_{1,2}$ are defined as the angles of the half-wave plates inserted in the paths along which signal 1 and signal 2 propagate, respectively. (b) Rydberg electromagnetically induced transparency (EIT). The horizontal axis stands for the detuning between the probe signal and the atomic transition from $5S_{1/2}$ ($F = 2$) to $5P_{1/2}$ ($F = 3$). In the experiment, the power of the coupling laser beam is 380 mW; beam size is ~ 19 μm. The probe beam has a beam waist of ~ 18 μm. (c) Time sequence for demonstrating entanglement. T is the memory time of entanglement.

$\mathbf{k}_S$ vector direction, where $\mathbf{k}_S = \mathbf{k}_{p1} - \mathbf{k}_{s1}$ is the wave vector of the low-lying atomic spin wave, $\mathbf{k}_{p1}$ and $\mathbf{k}_{s1}$ are the vectors of the pump-1 and signal-1 fields, respectively, and $\mathbf{r}_i$ denotes the position of the ith atom in the atomic ensemble. Through storing a signal-1 photon through Rydberg EIT [see Fig. 1(b)], a high-lying atomic spin wave $|a_{\text{high}}\rangle = 1/\sqrt{m} \sum_{i=1}^{m} e^{i\mathbf{k}_R \cdot \mathbf{r}_i} |1\rangle_1 \cdots |n\rangle_i \cdots |1\rangle_m$ is realized, where $\mathbf{k}_R = \mathbf{k}_C - \mathbf{k}_{s1}$ is the wave vector of the high-lying atomic spin wave, $\mathbf{k}_C$ is the vector of the coupling field, and $\mathbf{r}_i$ denotes the position of the ith excited Rydberg atom in the atomic ensemble. This type of spin wave involves a high-lying excited atom showing a special difference from a low-lying atomic spin wave; for example, the atomic size scales as $\sim n^2 \alpha_0$ (where α_0 is the bohr radius and n denotes the principal quantum number of the Rydberg atom). Finally, we establish the nonclassical correlation between the low- and high-lying atomic spin waves. In this process, in order to build up the nonclassical correlation between these two spin waves, small detuning ~ -10 MHz [see EIT spectrum in Fig. 1(b)] is used to match the $\sim +10$ MHz signal-1 photon. The reason to go off resonance is to reduce spontaneous-emission noise in the generating signal-1 field; the reason to not have larger detunings is to maintain the EIT visibility. The detected signal-1 photons before and after memory are shown in Fig. 2(a); the

storage efficiency after a programmed storage time of 300 ns is $\sim 22.9\%$. In principle, the storage efficiency can be further improved by optimizing the optical depth of atoms, the Rabi frequency of the coupling laser, the pulse profile of the signal-1 photon, the bandwidth matching between storage media and the signal-1 photon, etc.

To check whether or not the nonclassical property is retained during the storage, we map the low-lying and high-lying atomic spin waves to the signal-1 and signal-2 photons by opening the pump 1 and coupling pulses again after a programmed time, and check whether or not the Cauchy-Schwarz inequality was violated [18]. Classical light
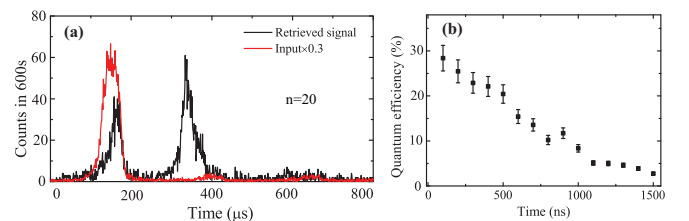

FIG. 2. (a) Detecting heralded signal-1 photons with storage time of 300 ns. The storage efficiency is 22.9%. (b) The memory efficiency vs storage time at $n = 20$.

satisfies $R = [g_{s1,s2}(t)]^2/g_{s1,s1}(t)g_{s2,s2}(t) \leqslant 1$, where $g_{s1,s2}(t)$ is the normalized second-order cross correlation between signal-1 and signal-2 photons, and $g_{s1,s1}(t)$, and $g_{s2,s2}(t)$ are the corresponding autocorrelation of signal-1 and signal-2 photons, respectively. In our experiment, $R \geqslant 43.2 \pm 7.3$ is obtained by using the measured autocorrelations $g_{s1,s1}(t) = 1.64$ and $g_{s2,s2}(t) = 1.80$, and the Cauchy-Schwarz inequality was strongly violated, clearly demonstrating the preservation of nonclassical correlation during the storage of the signal-1 photon in MOT B.

The storage efficiency against storage time is shown in Fig. 2(b). We estimate the dephasing time from Doppler decoherence is of ~ 4.28 μs when considering the vector mismatch, $\Delta k = k_{475} - k_{795}$, and the velocity of the excited Rydberg atoms of 0.276 m/s. Thus, the Doppler decoherence and the lifetime of the Rydberg state ($n = 20$, with lifetime ~ 5 μs) are not the main limitations. The additional dephasing may be contributed from the perturbation of external fields.

We also characterized the single-photon property of the signal-1 photon before and after storage by checking a heralded autocorrelation parameter $g_{s1;s1/s2}(t) = P_2 P_{213}/P_{21}P_{23}$, which is a Hanbury-Brown-Twiss (HBT) experiment on a triggered signal-1 photon [19,26]. P_2 is the count of signal-2 photons; P_{21} and P_{23} are the twofold coincidence counts between the signal-2 photons and the two separated signal-1 photons, respectively; and P_{213} is the threefold coincidence counts between the signal-2 photons and the two separated signal-1 photons. A pure single photon has $g_{s1;s1/s2}(t) = 0$ and a two-photon state has $g_{s1;s1/s2}(t) = 0.5$. Therefore, $g_{s1;s1/s2}(t) < 1.0$ violates the classical limit and $g_{s1;s1/s2}(t) < 0.5$ suggests the near-single-photon character. We obtained $g_{s1;s1/s2}(t)$ of 0.12 ± 0.02 of the input single photons and $g_{s1;s1/s2}(t)$ is 0.10 ± 0.01 of retrieved single photons, both close to zero, which clearly confirmed the preservation of the single-photon nature in storage, i.e., definitively showed a single high-lying atomic spin wave in MOT B. In Refs. [8,27], the input light field is a coherent light and a single high-lying atomic spin wave is prepared via Rydberg interactions within a blockade radius, which is confirmed by postdetecting the read-out photons. Here, the single high-lying atomic spin wave is achieved by absorbing the heralded single photon.

At first, we realized the which-path entanglement of a heralded high-lying atomic spin wave in a specially designed interferometer, which can be written as

$$|\psi_1\rangle = \frac{1}{\sqrt{2}}(|0_R\rangle|1_L\rangle + e^{i\phi}|1_R\rangle|0_L\rangle), \quad (1)$$

where subscripts L and R refer to the left and right optical paths in the interferometer, ϕ denotes the relative phase between these two optical modes, which is set to zero, and $|0\rangle$ and $|1\rangle$ denote the number of states of high-lying atomic spin wave, respectively. The entangled properties can be characterized by
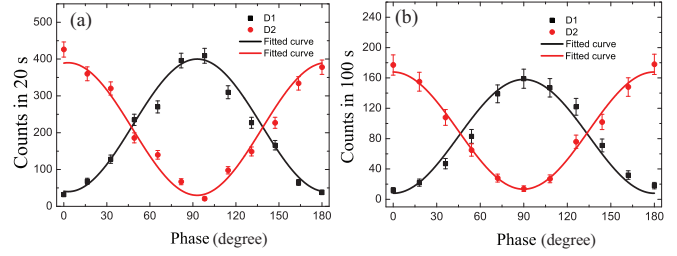

FIG. 3. (a) Single-photon interference between L and R paths. (b) Single high-lying atomic spin wave interference with different phases between L and R paths, which is controlled by changing the phase of the inserted phase plate (pp) which the signal-1 photon passes. These counts are conditioned upon detection of the signal-2 photon in path U. The visibilities of the interference curves in (a) and (b) are $90.6 \pm 0.4\%$ and $85.4 \pm 0.9\%$, respectively. The storage time is 300 ns.

the reduced matrix density r on the basis of $|n_L\rangle$ and $|m_R\rangle$ with $\{n,m\} = \{0,1\}$ [16]:

$$\rho = \frac{1}{P}\begin{pmatrix} p_{00} & 0 & 0 & 0 \\ 0 & p_{10} & d & 0 \\ 0 & d^* & p_{01} & 0 \\ 0 & 0 & 0 & p_{11} \end{pmatrix}, \quad (2)$$

where p_{ij} is the probability of finding i high-lying atomic spin waves in mode L and j high-lying atomic spin waves in mode R (see Table I); d is equal to $V(p_{01} + p_{10})/2$; and V is the visibility of the interference between modes L and R [see Fig. 3(b)]. Figure 3(a) is the input signal-1 interference between modes L and R. P is the total probabilities: $P = p_{00} + p_{10} + p_{01} + p_{11}$. To characterize the entanglement properties, we use the concurrence [28] Con $= \frac{1}{P} \max(0, 2|d| - 2\sqrt{p_{00}p_{11}})$, which takes values between 0 and 1 representing extremes corresponding to a separable state and a maximally entangled state. To obtain the concurrence of the entangled state corresponding to Eq. (2), we read the high-lying atomic spin wave into a single-photon state. We measured the different probabilities and calculated the concurrence to be $(3.39 \pm 0.5) \times 10^{-3}$ including all losses, thereby demonstrating the which-path entanglement of a high-lying atomic spin wave. The heralded probabilities are about 3.3×10^{-3} with overall optical losses of 94.6%, including photon-detection loss (50%), fiber coupling loss (30%), filtering losses 33.5% (two cavity filtering loss: 30%; one narrowband filter loss: 5%), and two-photon excitation loss (77%). In principle, these losses can be reduced significantly by improving the transmittance of the filters and the storage efficiency.

In order to demonstrate the entanglement between low- and high-lying atomic spin waves, we use a intrinsically stable interferometer consisting of two beam displacers (BD 1

TABLE I. Measurements of $\overline{p}_{ij}$ and concurrences C before and after collective Rydberg excitation.

	$\overline{p}_{00}$	$\overline{p}_{01}$	$\overline{p}_{10}$	$\overline{p}_{11}$	Con
$\overline{\rho}_{input}$	0.9516 ± 0.0008	$(2.61 \pm 0.04) \times 10^{-2}$	$(2.29 \pm 0.04) \times 10^{-2}$	$(2.6 \pm 0.4) \times 10^{-5}$	$(3.4 \pm 0.1) \times 10^{-2}$
ρ_{output}	0.9937 ± 0.0001	$(3.33 \pm 0.05) \times 10^{-3}$	$(2.98 \pm 0.05) \times 10^{-3}$	$(1.0 \pm 0.5) \times 10^{-6}$	$(3.39 \pm 0.5) \times 10^{-3}$

and BD 2) to prepare the entanglement between the signal-1 photon and the low-lying atomic spin wave in MOT A. In this configuration, due to the conservation of angular momentum in the SRS process, the signal-1 photons with two linearly angular momentums [labeled as U and D directions in Fig. 1(a)] entangle with the low-lying atomic spin waves encoded in wave vectors $\mathbf{k}_{S,U} = \mathbf{k}_{p1} - \mathbf{k}_{s1,U}$ and $\mathbf{k}_{S,D} = \mathbf{k}_{p1} - \mathbf{k}_{s1,D}$. The form of the entanglement is

$$|\psi_2\rangle = (|U_a\rangle|H_{s1}\rangle + e^{i\varphi}|D_a\rangle|V_{s1}\rangle)/\sqrt{2}, \quad (3)$$

with φ the relative phase between the upper and lower optical paths, which is set as zero in our experiment; $|U_a\rangle$ and $|D_a\rangle$ represent the low-lying atomic spin waves encoded in wave vectors $\mathbf{k}_{S,U}$ and $\mathbf{k}_{S,D}$, respectively. $|H_{s1}\rangle$ and $|V_{s1}\rangle$ denote the horizontal and vertical polarized state of the signal-1 photon, respectively. We next input the signal-1 photons into MOT B and subsequently stored it as a high-lying atomic spin wave. With the aid of a specially designed interferometer in MOT B, we established the entanglement between the low-lying atomic spin wave in MOT A and the high-lying atomic spin wave in MOT B, which can be expressed as

$$|\psi_3\rangle = (|U_a\rangle|r_L\rangle + e^{i(\varphi+\theta)}|D_a\rangle|r_R\rangle)/\sqrt{2}, \quad (4)$$

where $|r_L\rangle$ and $|r_R\rangle$ are the corresponding state of the high-lying atomic spin wave encoded in $\mathbf{k}_{R,L} = \mathbf{k}_C - \mathbf{k}_{s1,L}$ and $\mathbf{k}_{R,R} = \mathbf{k}_C - \mathbf{k}_{s1,R}$, respectively.

If considering the low- and high-lying atomic spin waves individually, the states of each spin wave are both mixed in K-vector spaces. However, the overall state of these two spin waves cannot be described independently; it is an entangled state. We checked this entanglement between them by mapping the atom-atom entanglement into the photon-photon polarization entanglement. By detecting the signal-2 photon in the polarization direction of $|H\rangle$, $|V\rangle$, $|H-V\rangle$, and $|H+V\rangle$, respectively, we record the coincidence rates between the signal-1 and signal-2 photons against the angle ϑ_1 of the HWP$_1$ through which the signal-1 photon passes, and plot the two-photon interference curves [shown in Fig. 4(a)]. All visibilities are better than the threshold of 70.7% that is the benchmark of Bell's inequality, showing that entanglement has been preserved during storage. We also used the well-known Bell-type CHSH inequality to check the entanglement. We define the S value as

$$S = \left| E(\theta_1, \theta_2) - E(\theta_1, \theta_2') + E(\theta_1', \theta_2) + E(\theta_1', \theta_2') \right|, \quad (5)$$

where ϑ_1 and ϑ_2 are angles of the inserted half-wave plates shown in Fig. 1, and the different $E(\theta_1, \theta_2)$ are calculated using

$$E(\theta_1, \theta_2) = \frac{\begin{array}{c} C(\theta_1, \theta_2) + C(\theta_1 + \frac{\pi}{2}, \theta_2 + \frac{\pi}{2}) \\ -C(\theta_1 + \frac{\pi}{2}, \theta_2) - C(\theta_1, \theta_2 + \frac{\pi}{2}) \end{array}}{\begin{array}{c} C(\theta_1, \theta_2) + C(\theta_1 + \frac{\pi}{2}, \theta_2 + \frac{\pi}{2}) \\ +C(\theta_1 + \frac{\pi}{2}, \theta_2) + C(\theta_1, \theta_2 + \frac{\pi}{2}) \end{array}}. \quad (6)$$

The angles are $\vartheta_1 = 0$, $\vartheta_2 = \pi/8$, $\vartheta_1' = \pi/4$, and $\vartheta_2' = 3\pi/8$. The S value we obtained is 2.29 ± 0.03. All experimental data including two-photon visibilities and the S value suggest that there is an entanglement between the low- and high-lying atomic spin waves. We also performed two-qubit tomography on the read-out photons of signal 1 and signal 2. The reconstructed density matrix [Figs. 4(a) and 4(b)], when compared
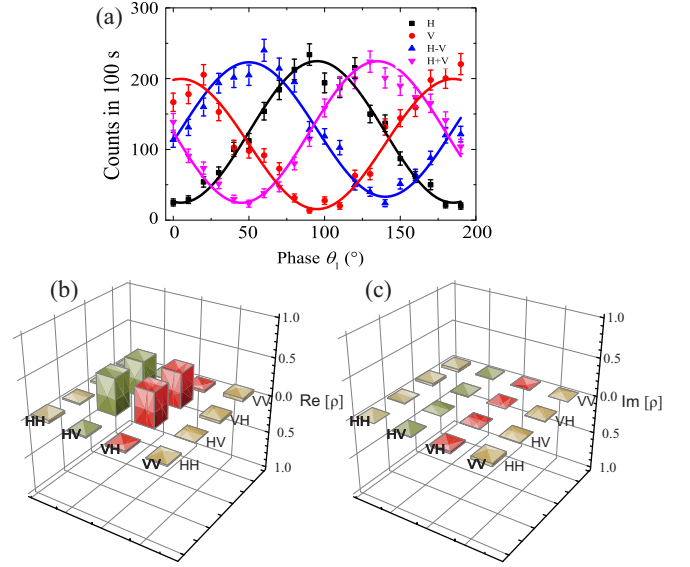

FIG. 4. (a) The coincidences between the signal-1 and signal-2 photons against the angle ϑ_1 of the half-wave plate (HWP$_1$) through which the signal-1 photon passes, where the signal-2 photon is detected in the polarization direction of H, V, $H-V$, and $H+V$, respectively. The interference visibilities are $84.2\% \pm 1.0\%$, $87.8\% \pm 0.8\%$, $82.3\% \pm 1.2\%$, and $81.6\% \pm 1.2\%$, respectively. (b) Real and (c) imaginary parts of the density matrices of the read-out entangled photonic state. The storage time is 300 ns.

with the ideal density matrix of the maximally entangled state, yields a calculated fidelity of $89.4 \pm 2.6\%$. We conclude again that entanglement between the low- and high-lying atomic spin waves existed in the separated atomic ensembles.

In summary, we reported on an experiment where we have constructed a hybrid interface between two disparate atomic systems. We have demonstrated two different entangled states in our experiment: which-path entanglement of a high-lying atomic spin wave and the entanglement between a high-lying atomic spin wave and a low-lying atomic spin wave. These two entanglements are totally different because they correspond to a single-particle and two-particle independently separated quantum state. The entanglement established between low- and high-lying atomic spin waves in two atomic ensembles is physically separated 1 meter apart. With the high-lying atomic spin wave being highly sensitive to external perturbations such as stray electric fields and blackbody radiation, this hybrid entanglement offers many prospective projects on sensing external perturbation. Moreover, via dipole interaction between the Rydberg atoms, one can in principle demonstrate blocking or switching photonic entanglement based on such system. Our results in establishing two atomic spin waves with different scales show promise for advances in the field of quantum information science and fundamental studies in quantum physics, especially in constructing Rydberg-based quantum networks.

[1] H. J. Kimble, Nature (London) **453**, 1023 (2008).

[2] A. Gaëtan, Y. Miroshnychenko, T. Wilk, A. Chotia, M. Viteau, D. Comparat, P. Pillet, A. Browaeys, P. Grangier *et al.*, Nat. Phys. **5**, 115 (2009).

[3] E. Urban, T. A. Johnson, T. Henage, L. Isenhower, D. Yavuz, T. Walker, and M. Saffman, Nat. Phys. **5**, 110 (2009).

[4] D. Jaksch, J. I. Cirac, P. Zoller, S. L. Rolston, R. Côté, and M. D. Lukin, Phys. Rev. Lett. **85**, 2208 (2000).

[5] M. D. Lukin, M. Fleischhauer, R. Cote, L. M. Duan, D. Jaksch, J. I. Cirac, and P. Zoller, Phys. Rev. Lett. **87**, 037901 (2001).

[6] M. Saffman, T. Walker, and K. Mølmer, Rev. Mod. Phys. **82**, 2313 (2010).

[7] L. Isenhower, E. Urban, X. L. Zhang, A. T. Gill, T. Henage, T. A. Johnson, T. G. Walker, and M. Saffman, Phys. Rev. Lett. **104**, 010503 (2010).

[8] Y. Dudin and A. Kuzmich, Science **336**, 887 (2012).

[9] O. Firstenberg, T. Peyronel, Q.-Y. Liang, A. V. Gorshkov, M. D. Lukin, and V. Vuletić, Nature (London) **502**, 71 (2013).

[10] L. Li, Y. Dudin, and A. Kuzmich, Nature (London) **498**, 466 (2013).

[11] S. Baur, D. Tiarks, G. Rempe, and S. Dürr, Phys. Rev. Lett. **112**, 073901 (2014).

[12] H. Gorniaczyk, C. Tresp, J. Schmidt, H. Fedder, and S. Hofferberth, Phys. Rev. Lett. **113**, 053601 (2014).

[13] C. Carr, R. Ritter, C. G. Wade, C. S. Adams, and K. J. Weatherill, Phys. Rev. Lett. **111**, 113901 (2013).

[14] D. Ding, C. Adams, B. Shi, and G. Guo, arXiv:1606.08791.

[15] L.-M. Duan, M. Lukin, J. I. Cirac, and P. Zoller, Nature (London) **414**, 413 (2001).

[16] K. S. Choi, H. Deng, J. Laurat, and H. Kimble, Nature (London) **452**, 67 (2008).

[17] A. Radnaev, Y. Dudin, R. Zhao, H. Jen, S. Jenkins, A. Kuzmich, and T. Kennedy, Nat. Phys. **6**, 894 (2010).

[18] A. Kuzmich, W. Bowen, A. Boozer, A. Boca, C. Chou, L.-M. Duan, and H. Kimble, Nature (London) **423**, 731 (2003).

[19] T. Chaneliere, D. Matsukevich, S. Jenkins, S.-Y. Lan, T. Kennedy, and A. Kuzmich, Nature (London) **438**, 833 (2005).

[20] H. Zhang, X.-M. Jin, J. Yang, H.-N. Dai, S.-J. Yang, T.-M. Zhao, J. Rui, Y. He, X. Jiang, F. Yang *et al.*, Nat. Photon. **5**, 628 (2011).

[21] D.-S. Ding, W. Zhang, Z.-Y. Zhou, S. Shi, G.-Y. Xiang, X.-S. Wang, Y.-K. Jiang, B.-S. Shi, and G.-C. Guo, Phys. Rev. Lett. **114**, 050502 (2015).

[22] D.-S. Ding, W. Zhang, Z.-Y. Zhou, S. Shi, B.-S. Shi, and G.-C. Guo, Nat. Photon. **9**, 332 (2015).

[23] L.-M. Duan and C. Monroe, Rev. Mod. Phys. **82**, 1209 (2010).

[24] R. Van Meter, T. D. Ladd, A. G. Fowler, and Y. Yamamoto, Int. J. Quantum Inf. **08**, 295 (2010).

[25] L. Yang, W. Jing-Hui, S. Bao-Sen, and G. Guang-Can, Chin. Phys. Lett. **29**, 024205 (2012).

[26] P. Grangier, G. Roger, and A. Aspect, Europhys. Lett. **1**, 173 (1986).

[27] D. Maxwell, D. J. Szwer, D. Paredes-Barato, H. Busche, J. D. Pritchard, A. Gauguet, K. J. Weatherill, M. P. A. Jones, and C. S. Adams, Phys. Rev. Lett. **110**, 103001 (2013).

[28] W. K. Wootters, Phys. Rev. Lett. **80**, 2245 (1998).